C-CORE Publication No. 90-3

Stationarity of acoustic intensity measurements on steel plates

Jacques Y. Guigné, Paul G. Williams, and John G. Adams
Centre for Cold Ocean Resources Engineering, Memorial University of Newfoundland, St. John's, Newfoundland A1B 3X5, Canada

(Received 6 April 1989; accepted for publication 9 January 1990)

The problem of identifying reproducible frequency bands useful for the nondestructive evaluation of steel plates using the dynamic acoustical intensity scanning concept (DAIS) is addressed. Reproducible frequency bands are essential so that subsequent changes in sound intensity patterns can confidently be attributed to structural changes rather than to random fluctuations. A number of evaluation methods are tried. Stationary frequency bands are identified by all methods in the range of 100–4000 Hz. The most sensitive and practical evaluation method is deemed to be the comparison of intensity versus time data collected separate from the plate scans. This method is accurate, convenient, and can be automated to exclude all unwanted frequency bands during testing. The remanent intensity factor technique, while useful in identifying stationarity, is less sensitive and more difficult to implement.

PACS numbers: 43.85.Fm, 43.40.Dx, 43.35.Zc

INTRODUCTION

A dynamic acoustical intensity scanning concept (DAIS) has been proposed and verified for the detection of fatigue cracks in offshore structures.[1–3] In this nondestructive testing technique, the measurement of sound intensity allows the mapping of the flow of acoustic energy through a structure. The energy flow patterns produced respond to the changes that occur in the structure over time. The resultant changes in the energy flow at certain frequency bands (called indicative frequency bands) clearly identify the presence of defects in the structure.

In previous work on the DAIS concept, the selection of the indicative frequency bands was based on the level (in dB) of the acoustic power spectrum that was calculated by integrating the intensity over the surface area of the grid at each frequency. Frequency bands showing levels higher than a determined cutoff, below which represents a pseudoreactive or environmental component, were chosen. Figure 1 illustrates this logic. In this example, 50 dB was chosen as the cutoff value.

This selection process is insufficient because of the nonstationarity in certain frequency bands. This has been observed from inspection of experimental data which show that some frequency bands exhibit significant changes over time even when structural properties are held constant. It is therefore essential that the frequency bands chosen be those in which the energy flow patterns are repeatable and hence give consistent results under constant conditions. Subsequent changes in these patterns can then be attributed with confidence to structural defects rather than to random fluctuations.

Although visual inspection can be used to identify stationary frequency bands, this method is time consuming and is limited by inherent subjectivity and a lack of quantitative results. This paper introduces two identification methods: the remanent intensity factor and the intensity-time variation. These are evaluated along with power spectra as alternatives to the visual inspection approach.

I. EXPERIMENTAL METHODS

A. Specimen

The test specimen used in the investigations was a rectangular plate fabricated from 19-mm-thick 1024 structural steel. A 4-mm-wide, 12.5-mm-deep notch machined into the specimen served as a calibrated defect. The plate dimensions are shown in Fig. 2.

B. Instrumentation

A servo-hydraulic test system was used to apply an axial static tensile load of 75 kN to the specimen. The specimen was then subjected to an additional pseudorandom load oscillating with a bandwidth of 10 kHz. Although this oscillating load was small (0.25 kN), acoustic energy was produced from the vibrations. This energy propagated through the actuator and linkage to the specimen where it became the target of the intensity mapping.

The instrumentation setup is illustrated in Fig. 3. The intensity probe consisted of two 1/4-in. microphones in the face-to-face configuration. Microphone responses were referenced to a pistonphone producing a calibrated sound pressure of 124 dB at 100 Hz. Control of the intensity analyz-

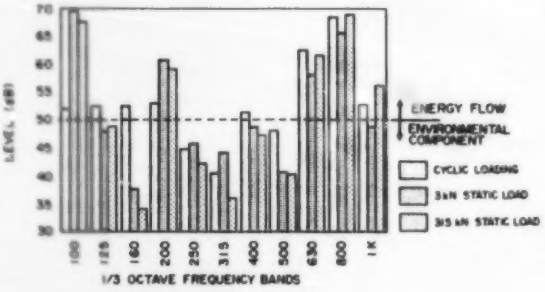

FIG. 1. Power spectra showing previous cutoff technique for determining indicative frequency bands [from Guigné *et al.*[1]].

 0001-4966/90/062773-06$00.80 © 1990 Acoustical Society of America

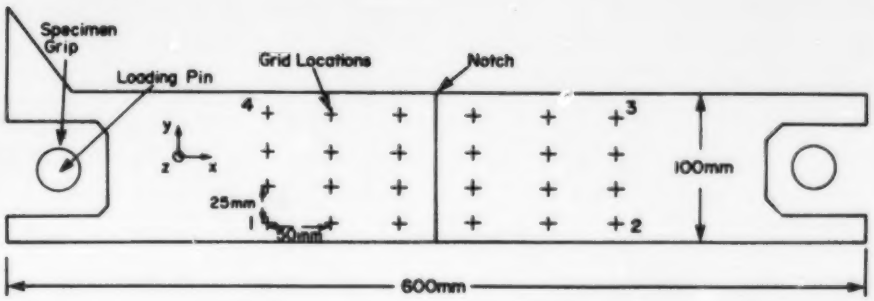

FIG. 2. Test specimen dimensions showing scanning grid.

er was carried out from the computer, which was also used for data storage and processing.

II. MEASUREMENT TECHNIQUE

A measurement grid of six rows and four columns was set up over the defect (see Fig. 2). At each grid location, a 1/3-octave-band intensity spectrum over the frequency range 100–4000 Hz was captured by the analyzer. The intensity probe was oriented to measure energy flow normal to the surface of the plate and was held with the acoustic center 25 mm from the surface of the plate. The use of a stand for the probe ensured consistent positioning and reproducible reflection characteristics. This mapping was carried out three times.

In addition to the intensity mappings, the time variation of the intensity spectra was also investigated. Twenty intensity spectra were recorded at intervals of approximately 2 s with a linear averaging time of 2 s. These readings were taken before each intensity mapping.

III. DATA PROCESSING AND RESULTS

Four methods of identifying stationary frequency bands were examined as follows.

A. Power spectra

The sound power spectra was calculated for each mapping of the plate. This was achieved by integrating the intensity over the grid area. A single level representing the sound power at each frequency for the entire grid resulted. The power spectra for three mappings are displayed in Fig. 4.

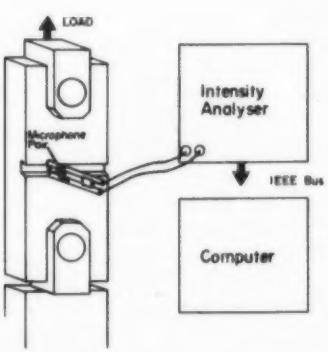

FIG. 3. Measurement setup.

B. Visual inspection

This correlation method involves a visual comparison between graphical plots made of the data for two mappings. The intensity mapping data are presented as three-dimensional surface maps for each frequency in the measured range, formed by interpolating the intensity levels between grid locations. These surface maps facilitate the visual comparison of data between trials. In addition, the contour map for each frequency is plotted over the measurment grid, and the intensity levels at the grid locations are displayed. Intensity levels that have a magnitude less than the 40-dB base level are omitted from these plots (treated as zero). Negative contours (the sign referring to a direction change) were plotted as broken lines.

Three classifications are used for the visual comparison: coherent, partial coherence, and no coherence. Figure 5 shows an example of the three-dimensional plots and contour map for the 2500-Hz frequency band of the first and second data mappings. This data pair is assigned a coherent visual comparison classification. Figure 6 shows a partially coherent pattern in the 800-Hz frequency band of the same data mappings. Figure 7 is an example of a noncoherent pattern, in the 400-Hz frequency band.

C. Remanent intensity factor

In an attempt to quantify the visual inspection technique, a remanent intensity factor was applied. This factor is the relative difference between the magnitudes of the intensity levels (in dB) measured over the same area. This energy difference is displayed as contour maps and as data maps that show the remanent factors at each grid location. A negative sign on the data maps indicates a directional change between the two mappings being compared. Figure 8 shows the remanent intensity factor contour and data maps for the same data that was compared visually in Figs. 5–7.

D. Intensity versus time

As an alternative to the above methods, a more direct approach of examining the variation of intensity with time was applied to find frequency bands displaying constant intensity levels. For each frequency band, the mean and stan-

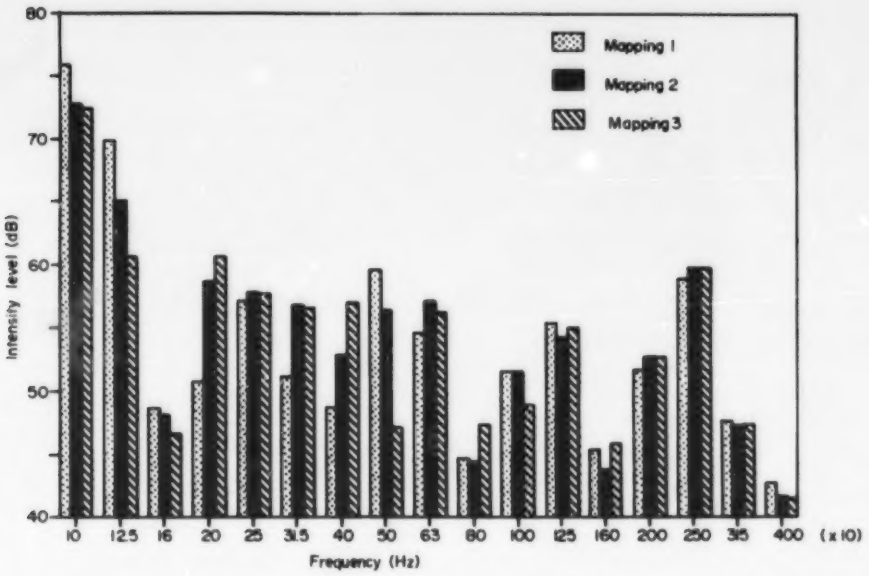

FIG. 4. Sound power spectra for three mappings of the same specimen.

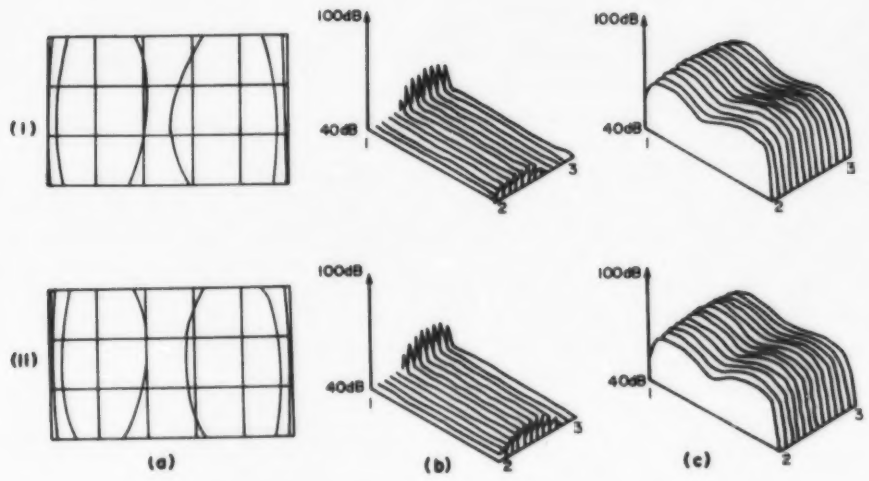

FIG. 5. Coherent energy flow patterns for mappings 1 (I) and 2 (II) at 2500 Hz. (a) Contour map, (b) three-dimensional plot of negative intensity, and (c) three-dimensional plot of positive intensity.

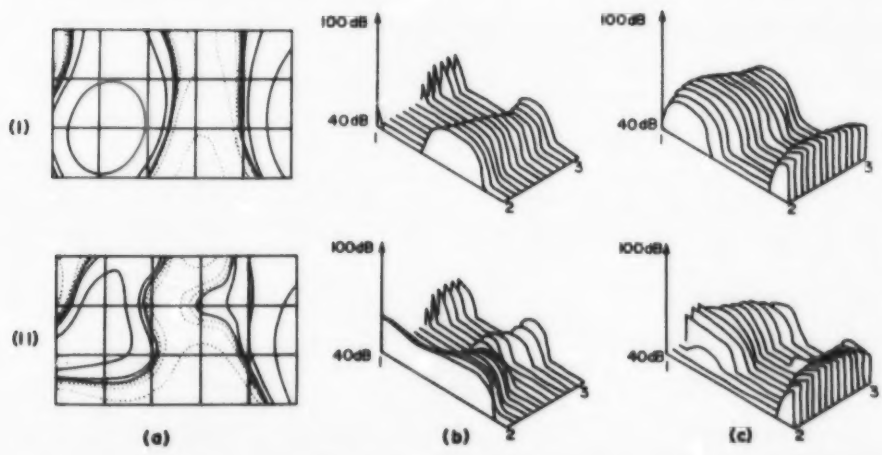

FIG. 6. Partially coherent energy flow patterns for mappings 1 (I) and 2 (II) at 800 Hz. (a) Contour map, (b) three-dimensional plot of negative intensity, and (c) three-dimensional plot of positive intensity.

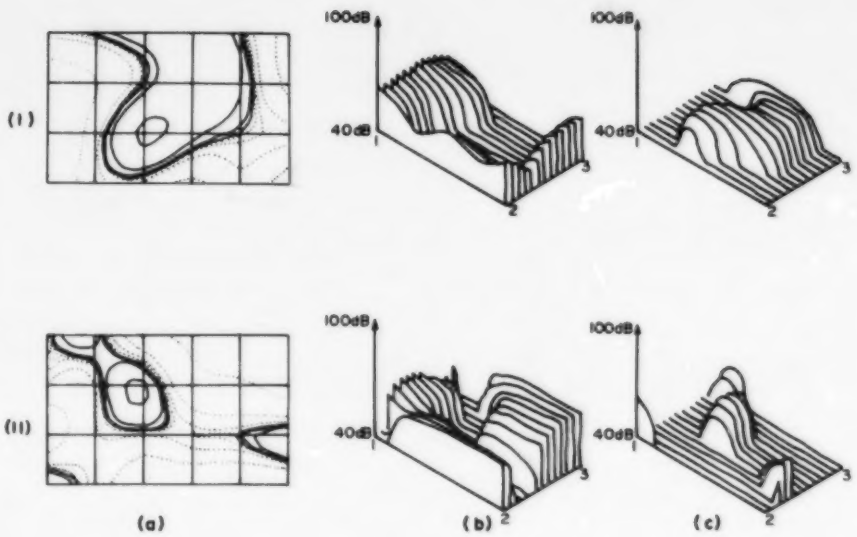

FIG. 7. Noncoherent energy flow patterns for mappings 1 (I) and 2 (II) at 400 Hz. (a) Contour map, (b) three-dimensional plot of negative intensity, and (c) three-dimensional plot of positive intensity.

dard deviations (s.d.) of 20 recorded points were calculated. The standard deviation was used as an indicator of the scatter of the points about the mean. The results are presented in Table I. Table II shows the average standard deviation over the three mappings alongside the visual inspection results. In the visual inspection columns, P represents partially coherent, C, coherent, and N, noncoherent.

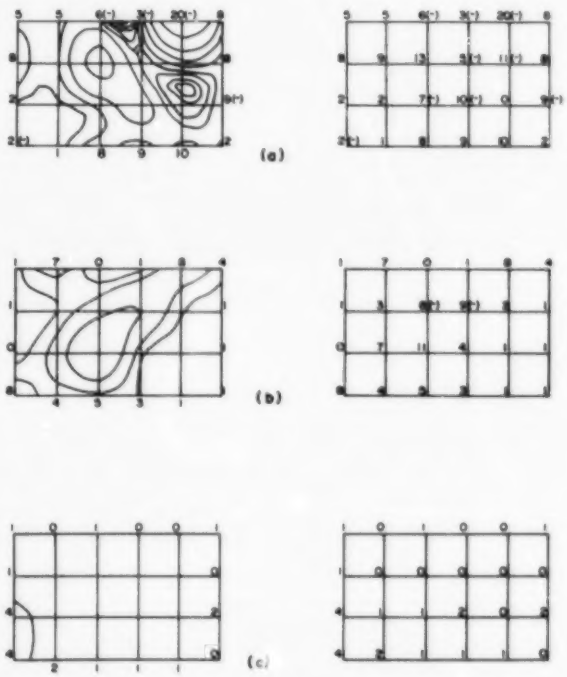

FIG. 8. Contour and data maps of remanent intensity factors calculated between mappings 1 and 2. (a) 400 Hz, (b) 800 Hz, and (c) 2500 Hz.

IV. INTERPRETATION

Examination of the power spectra (Fig. 4) reveals that, while the variation in each frequency band shows some correlation with the visual inspection results, the use of a cutoff level is invalid. For example, the 1600- and 3150-Hz slots, which show good visual correlation (Table II), are excluded with a cutoff of 50 dB, while the 125-, 200-, and 315-Hz slots, showing no visual correlation, are included.

The intensity versus time analysis provides a more sensitive method of highlighting these changes. Table II compares the average standard deviation to the visual comparison results at each of the frequency bands. From the data presented in Table II, Fig. 9 plots the frequency dependence of the standard deviations. In this figure, the results of the

TABLE I. Standard deviations and means for intensity versus time data.

Frequency (Hz)	s.d. Trial 1	s.d. Trial 2	s.d. Trial 3	Mean Trial 1	Mean Trial 2	Mean Trial 3
100	0.39	0.81	0.21	73.09	− 73.71	− 78.97
125	0.54	0.31	1.37	− 78.12	− 73.66	− 69.83
160	39.29	49.26	38.11	− 17.65	37.94	33.46
200	1.05	50.32	1.37	− 40.78	− 69.73	− 70.88
250	0.74	0.63	1.00	64.97	63.73	62.80
315	0.64	1.31	0.21	− 61.64	− 62.69	− 67.43
400	2.39	49.23	1.18	− 16.98	59.83	− 60.73
500	0.35	0.42	0.60	− 62.96	− 66.24	62.03
630	1.42	1.54	0.91	63.46	63.90	64.09
800	43.82	2.38	2.28	54.82	26.31	53.45
1000	0.20	0.28	0.30	− 65.00	− 64.33	− 63.88
1250	0.24	0.20	0.18	62.73	61.76	61.62
1600	0.41	0.38	0.47	56.23	56.43	57.19
2000	0.10	0.09	0.07	62.03	62.20	62.61
2500	0.06	0.10	0.11	68.87	68.98	69.40
3150	0.18	0.15	0.19	53.08	52.92	52.70
4000	0.15	0.25	0.29	46.88	45.90	45.22

TABLE II. Average standard deviation versus visual inspection.

Frequency (Hz)	average s.d.	Visual inspection between mappings 1 and 2	1 and 3	2 and 3
100	0.47	C	C	C
125	0.74	N	N	N
160	42.22	C	P	P
200	17.58	P	P	N
250	0.79	C	C	C
315	0.72	N	N	C
400	17.60	N	N	N
500	0.46	N	N	P
630	1.29	P	P	P
800	16.16	P	P	P
1000	0.26	C	C	C
1250	0.21	C	C	C
1600	0.42	C	C	C
2000	0.09	C	C	C
2500	0.09	C	C	C
3150	0.17	C	C	C
4000	0.23	C	C	C

visual comparison between mappings 2 and 3 are denoted by hatching on the graph. In all but two of the frequency bands, a standard deviation of less than 1 implies visual correlation.

Analysis of the remanent intensity factor data, while more complex, also yields useful results. The mean values for the remanent intensity factors are calculated at each frequency, and the frequency dependence of these values, for each set of remanent factors, is plotted in Figs. 10–12. Again, visual comparison results from Table II are included and are denoted by different hatch patterns on the graphs. Each graph was divided into three zones (A, B, and C) bounded by horizontal lines at mean values of 2 and 4. These zones, representing no coherence, partial coherence, and coherent correlation, respectively, parallel the results from the visual inspection reasonably closely. Anomalies do exist, however, that can be explained to some extent by the inability of this method to accomodate directional changes in the energy flow patterns.

V. CONCLUSIONS

Consistent mappings of acoustic intensity for the specimen have been obtained. For the most part, mappings are

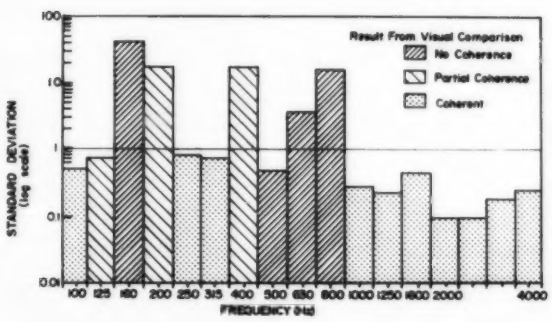

FIG. 9. Frequency dependence of average standard deviation values compared with visual inspection results between mappings 2 and 3.

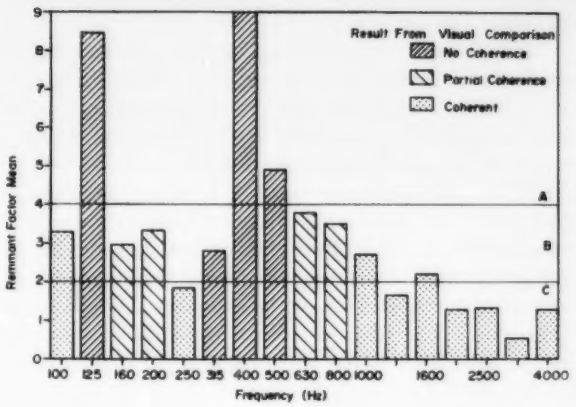

FIG. 10. Frequency dependence of remanent factor means and visual inspection results between mappings 1 and 2.

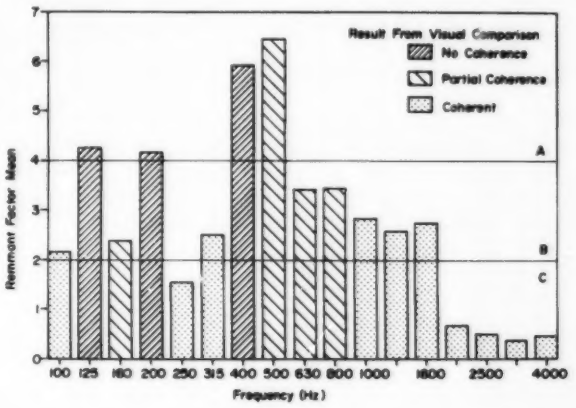

FIG. 11. Frequency dependence of remanent factor means and visual inspection results between mappings 1 and 3.

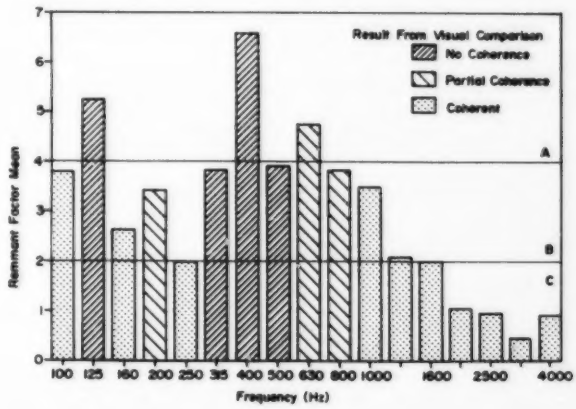

FIG. 12. Frequency dependence of remanent factor means and visual inspection results between mappings 2 and 3.

repeatable in the high- (1000–4000 Hz) frequency ranges and also at 100 and 250 Hz.

It has been shown that power spectra are not a suitable means of identifying indicative frequency bands. However, both intensity versus time and remanent intensity factors have been shown to be adept in this identification. For the purpose of stationary band detection in the DAIS system, the time variation of intensity method is easier to implement. One number eventuates from this type of measurement that characterizes the repeatability of the frequency band. By recording intensity versus time data before mapping a plate, unwanted frequency bands can be automatically ignored in the mapping. The remanent factor technique requires at least two scans of the plate and a critical comparison of the data sets before any conclusions can be made.

Ultimately, the use of the remanent factor and time variation of intensity methods serve to eliminate the subjectivity of visual inspection from the DAIS technique.

ACKNOWLEDGMENTS

Thanks are due to C-CORE for supporting this research, to NORDCO Ltd., and Dr. A. S. J. Swamidas (Memorial University of Newfoundland) for their interest, and to Dr. Robert Thompson and CANMET for encouragement and financial backing of the program. Thanks are also due to Desiree King for the diagrams.

[1] J. Y. Guigné, P. G. Williams, and V. Chin, "A Concept for the Detection of Fatigue Cracks in Welded Steel Nodes," Mar. Technol. **18**(4), 135–139 (1987).

[2] J. Y. Guigné, P. G. Williams, and V. Chin, "Analysis of the Deformation in a Partially Cracked Welded T-Plate," Mar. Technol. **18**(4), 141–143 (1987).

[3] J. Y. Guigné, P. G. Williams, and D. K. Mak, "Acoustical Imaging Using a DAIS Technique for Non-Destructive Testing," in *Acoustical Imaging*, edited by Hiroshi Shimizu, Noriyoshi Chubachi, and Jun-Ichi Kushibiki (Plenum, New York, 1989), Vol. 17, pp. 237–246.